

Bachelor's Thesis

Effizienzmessungen mit Modul-Prototypen für den ATLAS Pixeldetektor

Efficiency Measurements with Module Prototypes for the ATLAS Pixel Detector

prepared by

Fabian Sohns

from Hameln

at the II. Physikalisches Institut

Thesis number: II.Physik-UniGö-BSc-2014/07
Thesis period: 31st March 2014 until 4th July 2014
First referee: PD. Dr. Jörn Grosse-Knetter
Second referee: Prof. Dr. Arnulf Quadt

Contents

1. Introduction	1
2. The ATLAS Experiment	3
2.1. The ATLAS Inner Detector	4
2.2. Energy Deposition	5
3. Experimental Setup	9
3.1. Front End Read Out	9
3.2. USBpix System	10
3.3. The SUESS Probe Station and the Laser Injection	11
3.4. Communication With The Probe Station	12
3.5. Scan methods	16
4. Results	17
4.1. Alignment	18
4.2. Size of the Laser Point	19
4.3. X/Y direction measurements	21
4.4. The In-pixel Measurement	22
5. Discussion	25
A. Additional Plots	29

1. Introduction

The main task of particle physics is to check the Standard Model (SM) and to search for physics beyond the Standard Model. Because of this, the LHC (Large Hadron Collider) was built. It has a circumference of about 27 km and began operation in 2008. It is the largest particle accelerator on Earth [1]. The LHC is located at the research center CERN (Conseil Européen pour la Recherche Nucléaire) in Geneva [2]. After an upgrade of the center of mass energy from 7 TeV to 8 TeV in 2010, proton-proton collisions took place till its shutdown for further upgrades in 2013.

The SM predicts the properties of particles coming out of the collisions. These particles are detected and analysed by four experiments located at the four collision points of the LHC. One of them is the ATLAS experiment presented in the second chapter.

The LHC is going to be upgraded in the next 10 years to the so called High Luminosity LHC (HL-LHC). The aim is to increase the center of mass energy in the collisions to the maximal planned value of 14 TeV. Furthermore, the luminosity will be increased by a factor of five, and therefore, the data taken until the end of the run will be increased by a factor of 10 from 300 fb^{-1} , expected after the run in 2022, to 3000 fb^{-1} in 2035 [3].

In order to be able to collect all of this data, the ATLAS detector needs to be upgraded. In the first step, the Insertable B-Layer (IBL) was inserted in the ATLAS detector. It uses a new kind of read out chip, the FE-I4B instead of the FE-I3 currently used in the pixel detector. IBL improves tracking, vertex reconstruction and the b-tagging efficiency [3]. It was placed between the beam pipe and the Pixel Detector and is now the innermost part of the detector of which a short overview is given.

In the last step (about 2023), the whole Inner Detector will be replaced in order to cope with the harder radiation in this environment. To achieve the needed radiation hardness and to deal with all other challenges, new modules with new materials and new structures are built. To test these devices, under the aspect of radiation hardness and general performance, efficiency measurements are done. Enabling these efficiency measurements with laser injections is the main task of this thesis.

2. The ATLAS Experiment

The ATLAS (**A Toroidal LHC ApparatuS**) experiment is 45 metres long and has a diameter of 25 metres [4]. It is a nearly 4π detector (except for the beampipe). This means it detects particles in almost all directions from the interaction point, which is centered in the middle of the apparatus. The detector has different layers, each for measuring different properties of the particles flying through.

The Muon Spectrometer is the outermost part. It was built with an extra toroidal 1 T magnetic field to examine muons, the only particles besides neutrinos which do not deposited their energy at this point. The Muon Spectrometer is used for tracking, which requires a good spatial resolution and for triggering, meaning a good time resolution.

The second part of the detector is the calorimetry system consisting of an electromagnetic and a hadronic calorimeter where the energy of the particles is measured. In the electromagnetic calorimeter, electrons and positrons emit photons because of Bremsstrahlung. Photons can split up in electron and positron pairs. The primary particles shower and, due to these interactions, the energy of the particle can be measured. Under the assumption that a particle splits up into two other particles after an average radiation length X_0 , the shower length (in units of X_0), after which no particle has enough energy to split up again, can be calculated by

$$t_{max} = \frac{\ln \frac{E_0}{E_k}}{\ln 2} \quad (2.1)$$

where E_0 means the energy of the initial particle and E_k the critical energy for producing new particles [5, p. 135]. Due to this, the energy of the particle can be calculated by measuring the length of the shower in the calorimeter.

In the hadronic calorimeter the particles mainly interact with the nuclei of the material. The energy measurement principle is the same, but other effects need to be respected. In hadronic interactions more particles can be produced than in electromagnetic ones. Therefore, the number of particles in different showers fluctuates a lot.

In inelastic hadronic scattering it is very likely that a π^0 meson is produced which decays initially in two photons. This leads to an electromagnetic ratio in the hadronic shower

2. The ATLAS Experiment

which is not detected. Due to this, the energy resolution is worse than the energy resolution in the electromagnetic calorimeter [6].

2.1. The ATLAS Inner Detector

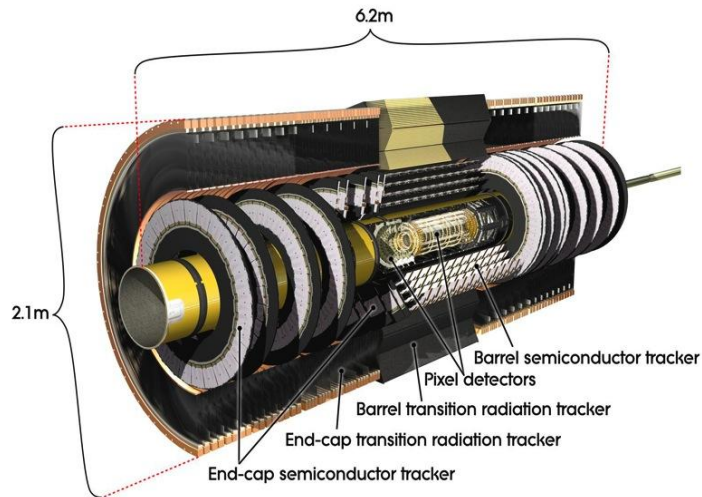


Figure 2.1.: The schematics of the ATLAS Inner Detector with the ATLAS Pixel Detector, the ATLAS Semiconductor Strip Tracker and the Transition radiation Tracker [4].

In the Inner Detector, shown in Figure 2.1, vertices can be reconstructed and b-quarks can be tagged by analysing the tracks of charged particles. These are bent due to a 2 T solenoid magnetic field, which allows for the measurement of momentum by calculating the Lorentz force and the centripetal force. To get a good track reconstruction, high spatial resolution is needed, because of the huge impact on further measurements.

In the Transition Radiation Tracker (TRT), the radiation sent out by particles passing the border between different materials is measured with a resolution of $130 \mu\text{m}$ in $r-\phi$ direction. It is particularly high for light particles like electrons and can therefore be used for a first particle identification. In the Semiconductor Strip Tracker (SCT), a grid of Silicon strip sensors allows for a high spatial resolution measurement with an intrinsic accuracy of about $17 \mu\text{m}$ in $r-\phi$ direction and of $580 \mu\text{m}$ in z direction.

In the pixel layer, Silicon sensors are used to receive a resolution of $10 \mu\text{m}$ in $r-\phi$ direction and $115 \mu\text{m}$ in z direction. In the current detector, 1744 n^+ -in- n sensor-chip-hybrid modules are used, which means that an n^+ pixel is placed in a n -type bulk with a p implant on the other side. The reason for this is the type inversion, a consequence of

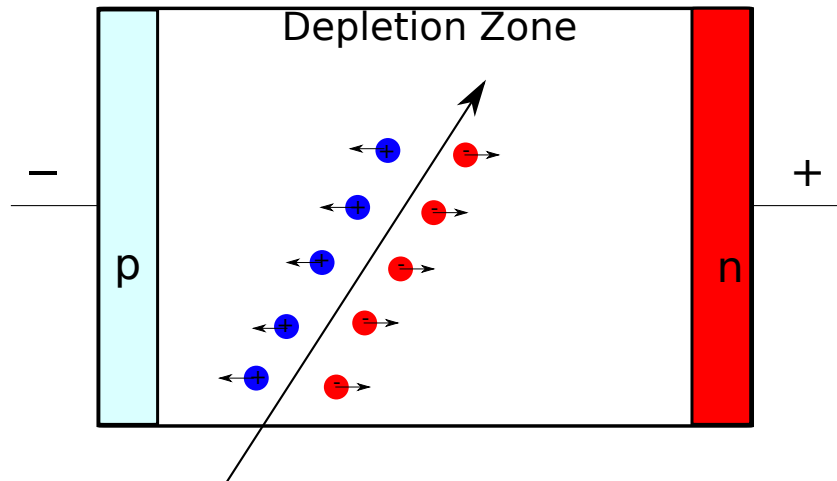


Figure 2.2.: Schematic overview over the charge production in the depletion zone of a semiconductor sensor.

radiation damage. This type of pixel can be used after the type inversion and for even higher radiation damage also under depleted [4].

To decrease the free charge carrier concentration and the leakage current, the Silicon needs to be doped. If an n and a p doped part are combined, the additional charge carriers of the doping can diffuse and recombine. Thus, a depletion zone is constructed in the interface region. Due to the recombination, there is a potential difference between the different doped parts and therefore an electrical field which stops the diffusion. By applying a voltage in reverse direction (n -doped side positive, p -doped part negative) the charge carriers are pulled to the electrodes and the depletion zone grows further [7].

A signal is now generated by the energy deposition of an incoming particle which produces electron-hole pairs as shown in Figure 2.2.

2.2. Energy Deposition

The interactions between particles and matter leads to free charge carriers which can be read out.

For photons, there are three different kinds of interactions. An overview of the different processes and their cross section is given in Figure 2.3. For lower energy (up to some keV), the Photoelectric effect is dominant. A photon is absorbed by a shell electron. If the photon energy is larger than the binding energy, the electron is free. With higher energy, the interaction probability for the Photoelectric effect decreases and the Compton Effect dominates. Here, a photon is scattered on a quasi-free electron and not absorbed. The transferred energy only depends on the angle of the deflection. The photon can now

2. The ATLAS Experiment

interact with other particles. For even higher energies, pair production is the dominating process. In this process, a photon splits up into an electron-positron pair. Due to momentum conservation, this only happens near a charged nucleus.

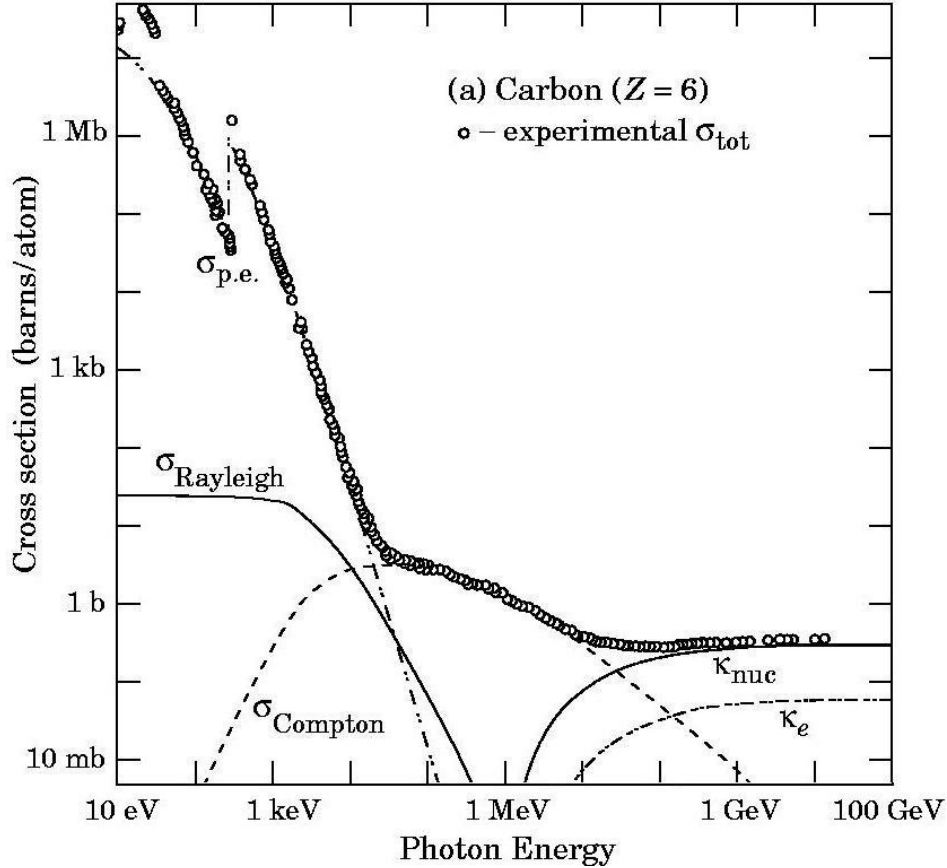


Figure 2.3.: Overview of the cross section for photons, depending on their energy with different dominating processes [8].

Besides photons, also charged particles interact with the detector material. The energy loss is dominated by ionisation. The Bethe-Bloch formular

$$\left\langle \frac{dE}{dx} \right\rangle = K z^2 \frac{Z}{A} \frac{1}{\beta^2} \left(\left(\ln \frac{2m_e c^2 \beta^2 \gamma^2 E_{\text{kin}}^{\text{max}}}{I^2} \right) - \beta^2 \right), \quad (2.2)$$

describes the average energy loss per distance and is shown in Figure 2.4 for muon with a positive charge.

$K = 0.307 \frac{\text{MeV cm}^2}{\text{mol}}$ describes a constant term, z the charge (in e) of the incoming particle, $\beta = \frac{v}{c}$ and $\gamma = \sqrt{\frac{1}{1-\beta^2}}$ the relativistic coefficients, I the average ionising energy of the material with atomic number Z and mass A , m_e the mass of an electron as well as $E_{\text{kin}}^{\text{max}}$

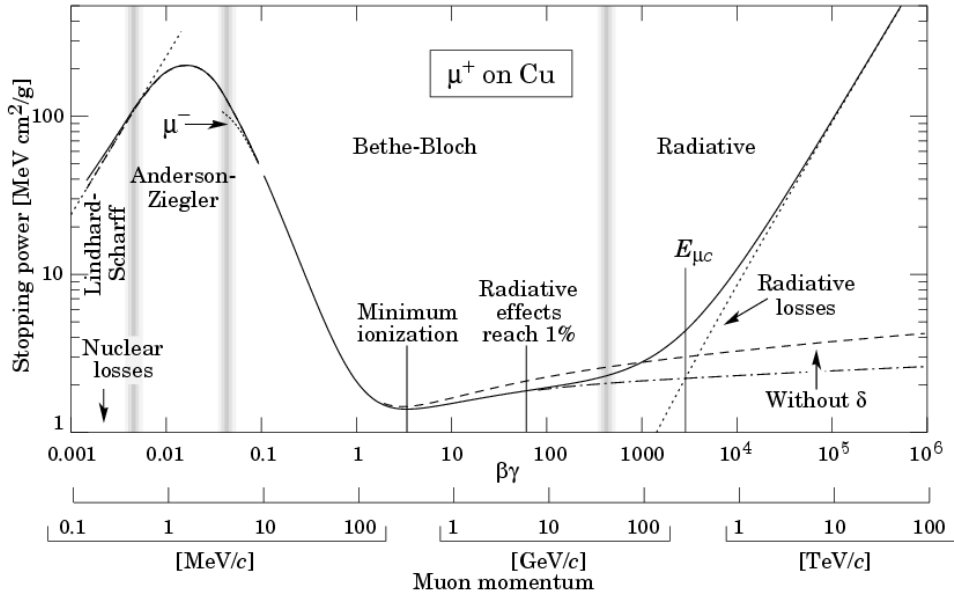


Figure 2.4.: The energy deposition for a μ^+ with the Bethe-Bloch area and corrections terms [8].

the maximal possible transferred energy per collision [7] [9]. For electrons and positrons the effect of Bremsstrahlung needs to be included in the formula. For higher energies, a mass correction term δ needs to be respected.

The minimal energy loss $\frac{dE}{dx} = 1.5 \left[\frac{\text{MeV}}{\text{cm}^2\text{g}} \right]$ is reached for $\beta\gamma$ about 3.5. Particles with this energy are called Minimal Ionising Particles (MIP). The energy of the particles produced in the LHC is higher than that of a MIP, but the energy loss just increases about a small factor. This is why MIPs are often used for lab measurements.

3. Experimental Setup

In this chapter, the setup for the measurement and the developments on it during the thesis are presented. In general, an efficiency measurement compares a known injected signal with the response of a module. This can be done with irradiated and unirradiated modules to compare the influence of the radiation or with new developed modules, to check if they work as supposed. There are different ways to do these measurements in a laboratory (radioactive source, laser,...). In this thesis, a laser is used for the injections. With the USBpix system, presented in this chapter, the signals are read out.

3.1. Front End Read Out

In the current ATLAS Pixel Detector, the Front End (FE) FE-I3 is used. Based on this, the FE-I4 was developed to deal with the higher detector occupancy due to the upgrade to HL-LHC. It is currently used in the IBL and is used to test the prototypes for HL-LHC. In addition, the used material and the power consumption was reduced. Furthermore, the digital read out was improved to allow a faster data transfer of 160 Mb/s [10].

The FE includes 26880 hybrid pixels arranged in 80 columns of 250 μm length and 336 rows of 50 μm width. Between the pixels, there are little gaps and on one side of each pixel is a wire bonding pad. Each pixel contains an own analog amplification stage, followed by a discriminator with an individual adjustable threshold. Only signals above this threshold are further processed as a hit, otherwise it is rejected as noise. Every pixel has its own read out directly on the sensor. This decreases the readout time.

If a hit occurs, the firing time of the discriminator is stored, and a latency counter is started. If the counter ends, the hit is discarded. Only when a trigger signal reaches the chip, the data is read out.

When a signal is generated, a capacitive charges itself and, when the signal stops, it is discharged by the feedback current. If a particle passes through the sensor, the Time over Threshold (ToT) can be measured. This is then equivalent to the generated charge

3. Experimental Setup

(Section 3.5). The formula to calculate the charge Q is

$$Q = a + b \cdot ToT + c \cdot ToT^2 + d \cdot ToT^3 \quad (3.1)$$

where a, b and c are parameters which are stored in the configuration [11].

The main source for inefficiency of the read out is the single pixel pile-up, which occurs, when a pixel is hit but, the discriminator is still high from a previous hit [12]. This effect occurs predominantly for a high rate of the signals.

For the measurements, the front end was located on a Single Chip Card (SCC). The SCC is a support card connected to the sensor and the FE by wire bonds. It is connected with an adapter card to the USBpix system via an ethernet cable. For the FE-I4A, a first version of the FE-14 which is used in the measurements, this adapter card contains the LVDS driver and the low voltage regulators.

3.2. USBpix System

Figure 3.1 shows the USBpix system used to communicate with the chip in test measurements via a PC. There are different adapter cards available. Thus, the Multi-IO-board and therefore the USBpix system can be used for different read-out devices.

The Multi-IO-board uses a micro controller to handle the scan routines and a Field Programmable Gate Array (FPGA) to send the commands to the FE and to store the data received from it on a Static Random Access Memory (SRAM) [13]. Furthermore, the FPGA enables the running of standard scans without communicating with a PC, which accelerates the processing time. A USB2.0 controller enables the transfer of data from and to the computer. 6 LEMO connections can be used to connect external triggers or power supplies. To send and receive signals from the Multi-IO-board, STcontrol is used. It is a graphical user interface based on ROOT and QT. It provides access to different classes based on the ATLAS PixLib package. With this interface, it is possible to load and set configuration data, handle the scan routines and to analyse the measured data with a data viewer [13]. The PixProber class allows communication with the probe station, in our case one manufactured by the company Süss. During this thesis, it was introduced to send commands which move the chuck or the scope to an arbitrary position and not only along a predefined wafer map.

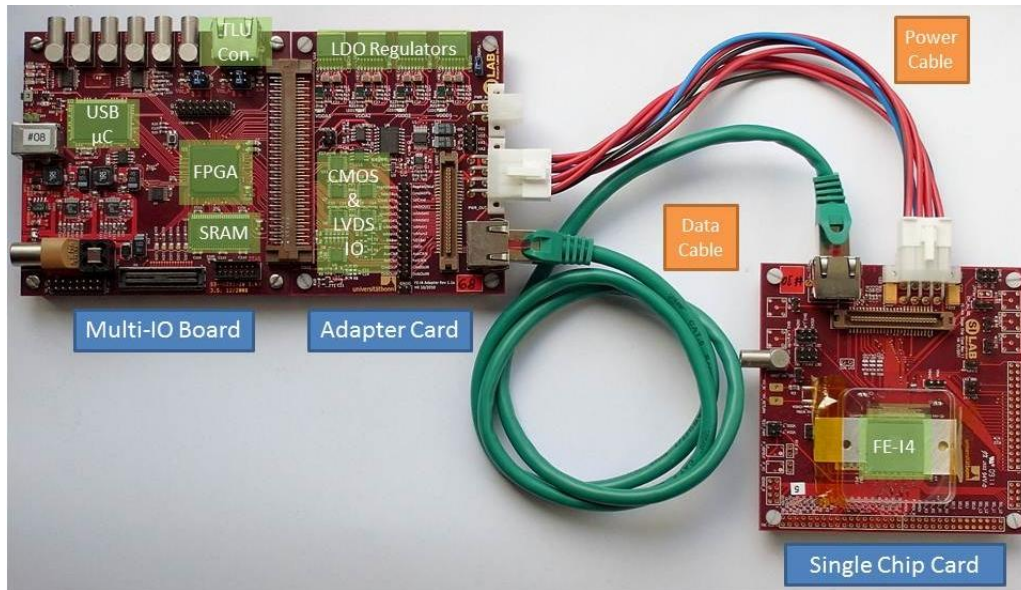


Figure 3.1.: The Multi-I/O board with the SCC which can be connected via an ethernet cable [13].

3.3. The SUESS Probe Station and the Laser Injection

The main part of the probe station PA300, used during this thesis, is a cased chuck. This can be cooled between -50°C and 160°C . A vacuum pump can prevent condensation in the case, as well as lock a module into position [14].

On top of the case, a microscope is installed. For this, different objectiv lens ($2\times$, $10\times$, $20\times$, $50\times$) are available. Both, the chuck and the scope, can be moved in three dimensions. For the measurements, a 671 nm red laser is chosen. For this wavelength, all of the photons sent out deposit their energy in the Silicon (*law of Bouger – Lambert*). The laser sends out pulses with a frequency of up to 1 MHz. With the laser, it is possible to send a known signal to the module. To regulate the intensity, resulting in different charges in the sensor, an attenuator is used. With a screw, a part of the laser beam can be absorbed. The attenuated laser beam is then injected into the microscope via an optical fibre.

In the microscope, the laser is split into two parts via a semi-permeable mirror. The first part is sent to a photodiode to measure the intensity, while the other one is focused on the chuck.

To move the scope or the chuck to an exact position, a wafer map can be constructed. On this map, specific positions are set to which the scope or the chuck can move. Since this map is not detailed enough to measure inside a single pixel, new commands for controlling

3. Experimental Setup

the devices have been programmed during my project. They allow the user to move the chuck and the microscope to an arbitrary position. To enable automatic measurements, they are included in the *PixProber* class and can be used via *STcontrol*, together with the standard scan methods.

3.4. Communication With The Probe Station

In this section, the connection between the different classes, used by *STcontrol* to control the probe station, is explained. A detailed description of the different classes is given in the paragraphs below.

To control the scans, different devices can be included in a configuration which stores the used settings (masking of pixels,...).

A *PixProber* has to be included as such a device in order to communicate with the probe station. For each device, different channels can be generated. These channels can be used to store set values (voltages, positions,...). For a *PixProber*, there needs to be a dummy channel which contains the informations to open the connection to the probe station (e.g. an IP-address). In measurements using the movement functions, there can be one channel for each axis to control. The axis is defined by the hardware (“Chuck” or “Scope”) and the direction (“X”, “Y”, “Z”).

By configuring the devices via *STcontrol*, a connection to the probestation is automatically established using the dummy channel.

STcontrol can scan over different parameters. In the Basic Parameters general settings like the trigger delay or the events per scan point can be set. In the scan parameters loops can be set over which the scan runs.

, For the position measurements, the *DCS_PAR*¹ are used as scan parameters. In the *DCS* control panel of the scan, a channel and the measuring type (here *position*) can be set.

For every scan point in a position measurement, the function to move the chuck or the scope is called, the position is given back and then the measurement is done. For each type of probe station there are specific commands, e.g. to move the chuck or to read the position. For the given probe station the class *OpenSuessPixProber* was used, which defines the type of the *PixProber* included in *STcontrol*.

By creating a channel, a new *PixProberDcs* object for the given type is generated. This includes the axis to control which are stored in a configuration for the channel.

Every *PixProberDcs* object knows an object of the *PixProber* class, in this case an

¹Detector Control System Parameters

OpenSuessPixProber. The functions of *PixProberDcs*, and therefore every channel, are called by STcontrol and transfer the command to the PixProber they know. If, for example, the initialisation is called, the connection to the probestation is opened by using the function *initHW* with the given IP address.

The final implementation to communicate with the probe station (to move the chuck or the scope and to read their positions) have been implemented in the class *Suess*. To read out the position two new the data types, *ReadChuckPositionResponse* and *ReadScopePositionResponse*, were implemented. They store the response of the probestation in a variable. This can then be accessed by the class *OpenSuessPixProber* which translates it into a position for every axis. This is then returned to the appendant *PixProberDcs* object, and with this, to the channel. An overview over the connection between the classes used for the communication between STcontrol and the probe station is given in Figure 3.3.

PixDcs-Class. The *PixDcs* class is the main class which is called when a channel is generated. It provides different functions which need to be implemented by subclasses. If the constructor of the *PixDcs* class is used, a type for the object is requested. For the type *PixProberDcs*, which is equivalent to the invoked class, a new object of this type is generated. Here the functions are implemented.

One function is the initialisation. Here, the layout of the channel used by STcontrol is generated. Using the *config* class, two menus to choose between *Chuck* and *Scope* and their positions are generated.

Two other functions which work similiar are the *ReadParam* and the *SetParam* functions. They are called by STcontrol for every scan point. If this is the case, the function checks which axis the dedicated channel controls. For *ReadParam* then the position is read out, for *SetParam* the new position is set. This is done, by using the included *PixProber* object and calling the implemented functions.

PixProber-Class. The *PixProber* class itself only contains the general mask for the functions subclasses need to implement comparative to the *PixDcs* class. This is done to allow the implementation of different types, but allowing external classes to use the same constructor for all of them.

For the *OpenSuessPixProber* class several functions to move the chuck using a wafer map are included as well as the movement and read out functions for an arbitrary position, which were implemented in this thesis. The structure of the functions included is quite similiar. All of them know an object of the class *Suess*. From this, the functions can be

3. Experimental Setup

called with default values.

Suess-Class. The class *Suess* is located in the libSuess package. It handles the communication between the computer and the probe station.

For this, the function *clientCommand(cmd, data)* is used. The variable *cmd* is the command to send to the probe station via the TCP/IP connection. A list of available commands can be found in the manual (e.g. *MoveChuck* or *MoveScopeZ*). The variable *data* contains the needed information for the command and is generated by the parameters with which the function is called. For the movement, the speed of the movement (default: 100%), the reference point (default: home position), the unit (default: micrometers) and a comp. level (default: Default) are written into *data*. An example of a command is given in Figure 3.2

```
void ProbeStation::MoveChuckZ(float z, char PosRef, char Unit, float velocity, char comp){
    stringstream data;
    std::string cmd = "MoveChuckZ";
    data << std::fixed << std::showpoint << std::setprecision(2) << velocity << " ";
    data << z;
    data << " ";
    if (PosRef=='H' || PosRef=='Z' || PosRef=='R')
    {
        data << PosRef;
        data << " ";
    }
    else throw Exception("Suess::ProbeStation::MoveChuck: Wrong reference point.");

    ... check for every variable if it contains an expected value, here shown for the reference point

    Response r(clientCommand(cmd, data.str()));
    r.validate(m_client_id);
}
```

Figure 3.2.: An example of a command in the class *Suess*, called by *OpenSuessPixProber*. It sends the command to move the chuck in the direction *z* with extra settings to the probestation via TCP/IP.

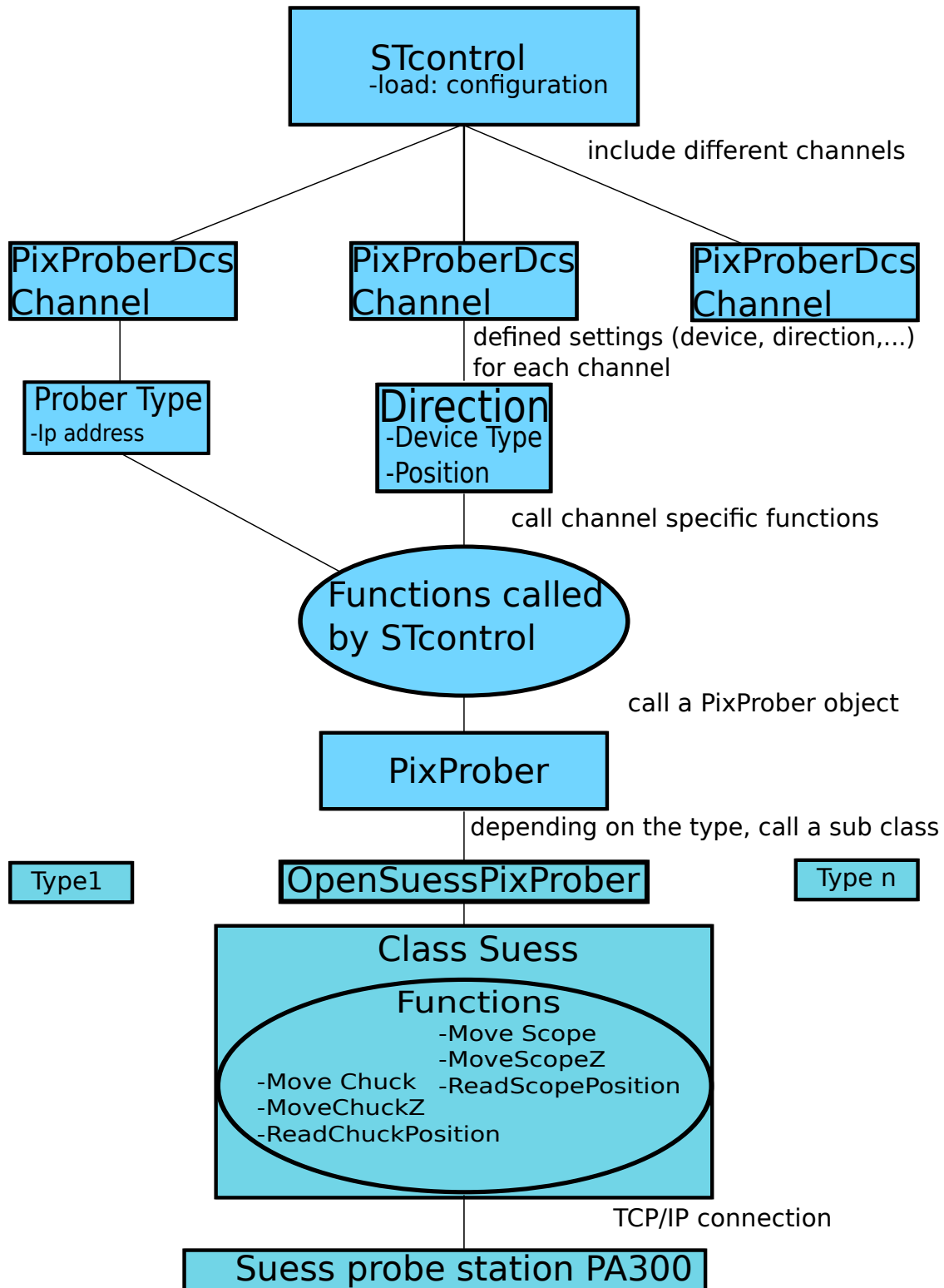


Figure 3.3.: Overview of the connection between the objects to communicate with a probe station. The class Sues is the final class to call the Probestation. It is included in the OpenSuessPixProber, a subclass of PixProber. It handles the response of the probe station such as the position. A PixProber is included for every PixProberDcs channel with a specific type. This type can be the direction and the device type or the general setting for the probe station type with the IP-address. For these channels similiar functions can be called by STcontrol.

3.5. Scan methods

There are different standard scans available for the USBpix system. In the following, the scans needed for the measurements are explained.

Analog and Digital Test. With these tests, it can be checked if the pixels work as expected. Furthermore, the connections of the testing apparatus can be checked, because the scans do not take a long time and give an overview over the whole module. Via an internal charge injection circuit, a defined amount of charge carriers can be injected in the discriminator (digital test) or the amplifier (analog test). The measured occupancy on each pixel should be the same as the injection. The pixels are organized in double columns. Since not enough charge can be generated for all pixels at the same time, by default, only every sixth pixel gets a signal from the injection. By shifting the selected pixel six times, a whole double column can be scanned.

Threshold Tuning. In order to distinguish between noise and signal, a threshold can be set for the pixels. The threshold is controlled by different DAC (Digital Analogue Converter) values. In the first step, the GDAC tuning, the threshold can be set for all pixels at the time by the global parameter GDAC. This is done by injecting a charge corresponding to the threshold to the pixel cell. For a fixed number of injections, the value for the threshold is adjusted if more than 50 % of the measured hits are above or below the threshold. Because of differences between the single pixels, the threshold needs to be set for each pixel individually. This is done by the TDAC tuning, which works similar to global adjusting [11].

In the FDAC tuning, the feedback current per pixel is set. This results in a correlation between the collected charge and the ToT, e.g. a ToT of 7 can be equivalent to a charge of 14,000 electrons.

Source Scan. Instead of injecting charges from an internal circuit, the scan expects an external source like a laser. This sends a trigger signal which then tells the read out electronics when a hit is expected. This ensures that the hits detected generated at the expected time.

To know which signal is expected, the *EventsperScanpoint* can be set as number of trigger signals. With this, for every trigger signal a hit should be detected and so the number of trigger signals is the expected result.

4. Results

The aim of the measurements is to check the programmed control, and to see how good the resolution of the efficiency measurements with the laser injection can be. Therefore, a FE-I4A with a $200\ \mu\text{m}$ n -in- p sensor was used. The sensor has a metallisation on the backside, which has two holes, one in the middle and one on an edge of the sensor. Here, the middle one was used (Figure 4.1). There are several pixels, each with a size of $250 \times 50\ \mu\text{m}^2$, available to be tested.

The microscope is focussed visually with the remote control at the probe station related to the metallisation. The trigger reaches the FE with a delay. This delay needs to be tuned. Therefore, the scan parameter can be set as “TRIGGER_DELAY”. With this setting, for every scan point a different delay of the trigger signal is used. Only for the right delay, a signal can be seen in the data. A first rough measurement with 10 delay steps showed hits by 20 and 30 steps, a detailed one in the range of 18 to 34 steps, so a delay of 30 was set. Furthermore, a LVL 1 can be set. This is the length of the periode in which signals are accepted by the read out. The standard settings used here are 16 clock signals. Each clock signal has a length of 25 ns.

The configuration was tuned for 14,000 injected electrons with an TOT of 7. It is specific to the used module, and includes masking of pixels and other specific settings. By default, the used configuration includes the analog and the digital voltage control. A PixProber was included as explained in Chapter 3.4. The intensity of the laser was tuned so that the ToT peaked at 7 as the configuration was tuned for this. If the intensity is chosen too low, the increase or decrease during a ToT scan would be smaller. The photo diode then measured a voltage of 1.5 V which is equal to 5672 electrons induced in the material. For the calculation equation 3.1 was used with the parameters $a = (1.15 \pm 0.01) \cdot 10^3$, $b = (6.297 \pm 0.005) \cdot 10^2$, $c = (2.171 \pm 0.006)$ and $d = (1.98 \pm 0.03) \cdot 10^{-3}$.

The parameters for the calculation were tuned for a frequency of 100 kHz. Since in the measurements 200 kHz were used, the number of injected electrons needs to be doubled so that $(11,344 \pm 14)$ electrons are assumed to be injected.

To test the programmed control three measurements were done with one alignment. For each measurement a pulse frequency of 200 kHz was chosen. The readout was set to wait

4. Results

Metal opening in the center

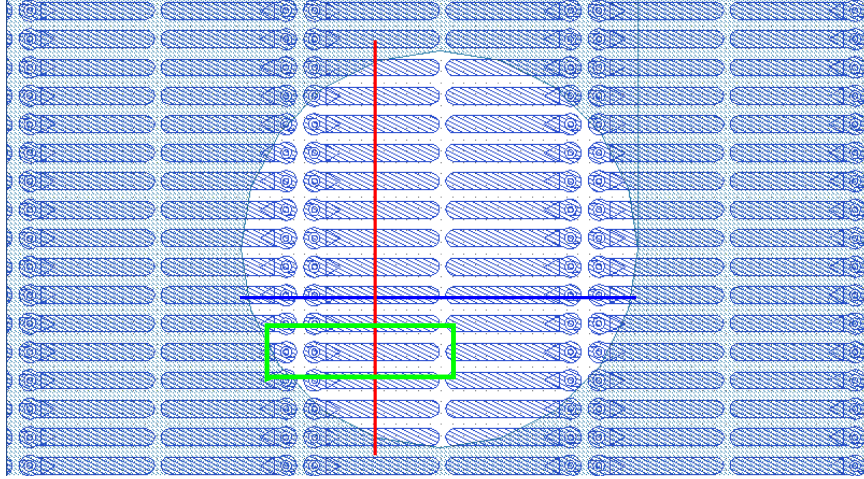


Figure 4.1.: The pixels on the sensor with the metallisation and the hole being used for test measurements. The coloured lines show the area for the measurements.

1000 trigger signals, so 1000 is the expected value of hits. The error for each measurement point is \sqrt{x} , since the data are Poisson distributed.

4.1. Alignment

For the measurements, the SCC was placed on the chuck and then connected to the Multi-IO-board laying in the probe station. To make precise measurements, the axis of the movement needs to be parallel to the axis of the pixels. The measurements are done with one setup, so the alignment needs to be done once to have similar condition for all measurements.

To align the module with the movement, the edge of the sensor was approached. This edge is parallel to the pixels, which can not be seen, and can therefore be used for the aligning. For this, a position on the edge was chosen, and then the first mark for the chuck was set. Moving the scope to a second position on the edge and setting the second mark causes the alignment function to spin the chuck.

Before every measurement, the imprecision of the alignment was measured by moving the scope on the edge of the sensor, note the x and y position, move the scope just along the x direction and then, after a few micrometers, note again the position. Now, it can

Measurement	number Movement in X [μm]	Difference to the edge [μm]	Percentage
1	200	8	4
2	200	7	3.5
3	200	8	4
4	200	6	3
5	200	7	3.5
6	400	17	4.25

Table 4.1.: The results for the imprecision for the alignment, measured before every measurement.

be seen that the scope moved away from the sensor edge. This distance is measured by moving the scope back to the edge and noting the difference in the y direction. The measured values are shown in Table 4.1. The uncertainty is estimated to be $1 \mu\text{m}$, since the precision of the movement of the scope is limited (see “Service Programs help” in the manual).

The SCC is held on the chuck via a vacuum pump but because of the geometry of the chip holder only on one point. A movement of the chuck could therefore spin the SCC which leads to a misalignment during the measurement. Hence, the scope was chosen to be moved.

With this settings four measurements were done, two over the hole along the x-axis at which for one the ToT was measured, one over the hole along the y-axis and one over a whole pixel. The efficiencies can be calculated by dividing the measured values by the expected signal. In the figures the total values are shown but the behaviour of the efficiency can be seen.

4.2. Size of the Laser Point

The intensity of the laser spot is assumed to have a Gaussian distribution. In this thesis, the size of the laser spot is defined as the area of the distribution which suffices to show hits in the pixel (Figure 4.2). For a certain intensity on the laser spot this can be seen through the microscope. The seen size of the laser spot increases with a higher intensity. Because of the Gaussian form of the laser spot not the size itself increases, only the part recognised by the microscope. Therefore, the size of the laser spot cannot be measured visually but with an extra measurement. The step size was chosen to be $1 \mu\text{m}$ along the x axis in the interval of $[-100, 500] \mu\text{m}$ from the home position of the x and y direction. Since the settings are the same for all measurements, especially the focus of the microscope, the diameter is the same for all measurements.

4. Results

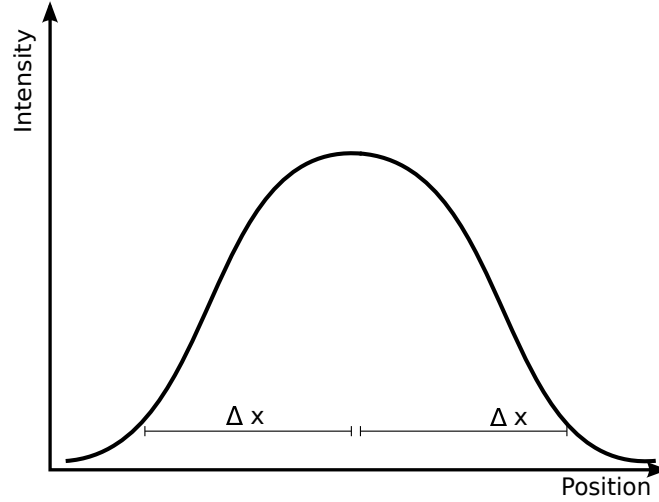


Figure 4.2.: The assumed Gaussian distribution for the laser intensity with the additional measured pixel size Δx .

Measured Spot Size. The diameter was calculated as suggested by M. Pfaff [14]. Therefore the ToT was plotted against the position in x direction for two different pixels fully passed during the scan (Figure 4.3). The width of the increase is a rate for the diameter of the laser spot. The ToT starts rising when the outer part of the laser hits the pixel and the intensity is high enough such that the threshold is reached. When the whole spot is over the pixel, the maximal ToT is reached and it falls again when the laser leaves the pixel. Therefore, the diameter d of the laser spot can be calculated by

$$d = P - A \quad (4.1)$$

where P is the position where the maximum is reached and A the position of the first hit. The second method is to use the first position and the last position where a hit is measured. On the first position the one side of the spot and on the last position the other side hits the pixel. Then d is therefore

$$d = A - B - D \quad (4.2)$$

where A and B are the positions of the first and the last hit and D is the length of the pixel. The values for the measured diameters seen in the plot are listed in Table 4.2. From this consideration and calculating the arithmetic average a diameter of $40 \mu\text{m}$ is assumed for the measurements. The error for the reading of the position is assumed as $5 \mu\text{m}$. From this, the error of the diameter derived to be $10 \mu\text{m}$.

Measurement	Position A [μm]	Position B [μm]	Position P [μm]	Diameter
1	-95	190	-	35
2	160	445	-	35
3	-95	-	-55	40
4	160	-	210	50
5	-	190	140	50
6	-	445	405	40

Table 4.2.: The size of the pixel calculated by the equations 4.1 and 4.2 for a length of $d = 250 \mu\text{m}$ for the pixel.

4.3. X/Y direction measurements

The one dimensional measurements were made along the Y-axis (Figure 4.1, red line) and the X-axis (Figure 4.1, blue line). Before starting, test measurements have to be made to exclude the testing range to be on the edge of a pixel or between two pixels, and to see if all pixels respond if they get a hit. Therefore, a larger step size was than chosen for the detailed measurement. The scope was positioned to the starting point where a measurement with 11 steps along the measurement range ($650 \mu\text{m}$ for the x and $600 \mu\text{m}$ for the y measurement) was started. With data viewer it can be seen, if the column/row (depending on the orientation of x and y) of the pixels hit stays the same for all steps. If this is the case, the measurement can be started since the whole range covers one y position. If not, the alignment needs to be checked or, depending on the size of the deviation, a new home position can be set, centered more on the pixel.

From these measurements it can be seen that all pixels along the x direction show hits (step size is smaller then the length of the pixel), for the y direction an extra measurement was started with a little smaller step size (step size was $60 \mu\text{m}$, pixel width is $50 \mu\text{m}$). The result for one single pixel for each measurement is shown in Figure 4.4.

In the appendix A, the plots for all single pixels are shown.

It can be observed that there is a sharp edge on which the occupancy for the pixels rises. Furthermore, there is an overlap between two neighbouring pixels. This appears when the size of the laser spot is larger then the gap between the pixels. Then both pixels get hits for the same step and for the same amount of trigger signals. That is why for one step there can be more then 1000 hits in total. The overlap is seen for about 17 steps on each edge which corresponds to $34 \mu\text{m}$. This corresponds to the calculated size of the laser spot.

4. Results

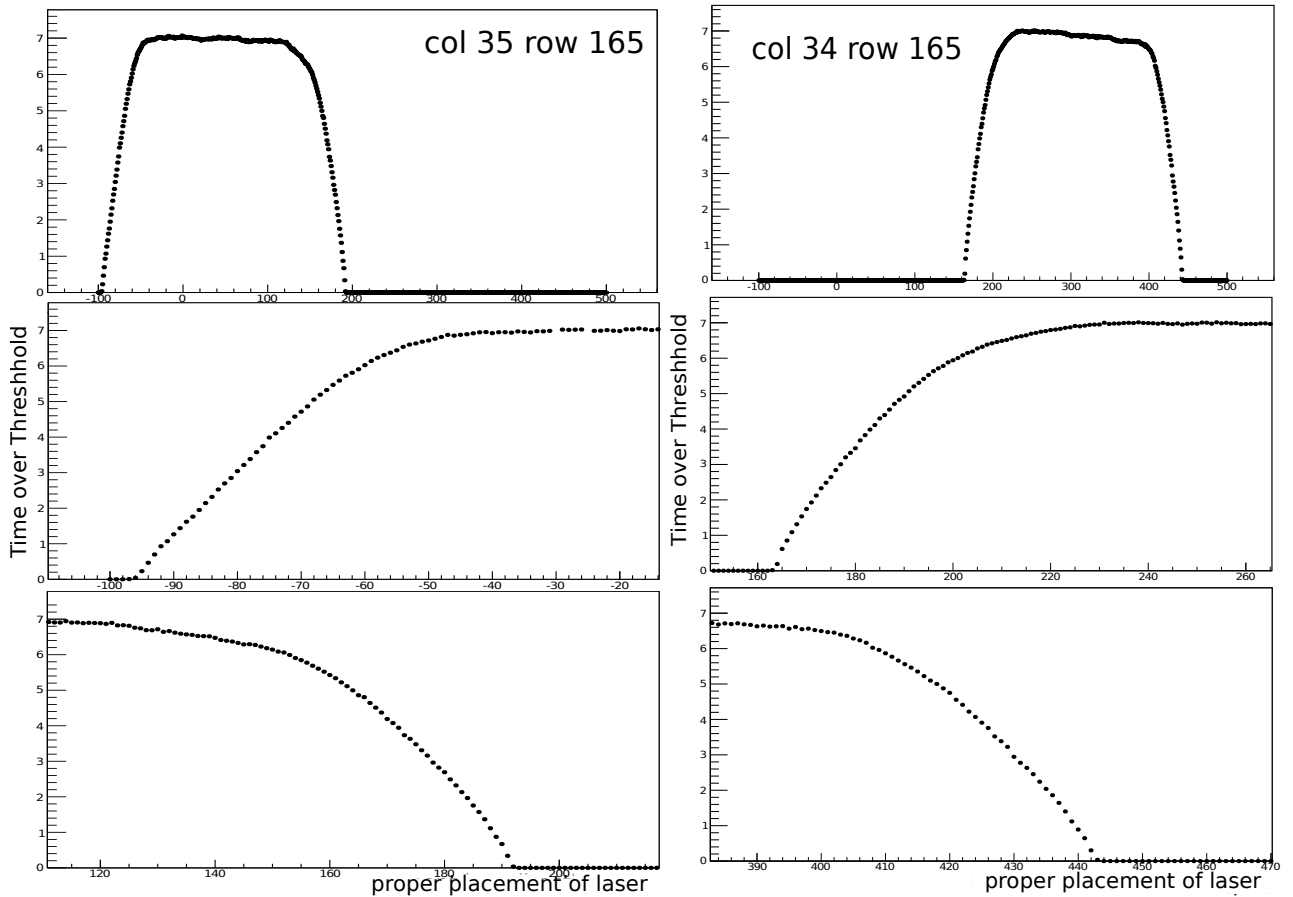


Figure 4.3.: The ToT for the pixels 34/165 and 35/165 as a function of the position. The lower pictures show the raising and the falling edge of the upper one.

4.4. The In-pixel Measurement

The two dimensional measurement was done along the x and the y axis (Figure 4.1, green line). For this measurement, the range needed to be adjusted. Therefore a position on the hole was chosen where a pixel edge can be expected from the schematics. The chosen pixel was on the row 35 and the column 165. Then, some measurements along the x axis were done to know where the neighbouring pixels begin and where the chosen pixel does not show hits anymore. Afterwards, the same was done for the y direction.

The chosen area was between the x coordinates $[-60, 56] \mu\text{m}$ and the y coordinates $[-130, 250] \mu\text{m}$ with respect to the chosen home position. At these coordinates an overlap is included to get a good view of the edge. The result is shown in Figure 4.5. The positions are shifted so that the starting point of the measurement lays in the origin. The form of the pixel can be seen as expected from Figure 4.1. An influence of the bias dot cannot be seen since the occupancy in the center region is homogenous to the maximal

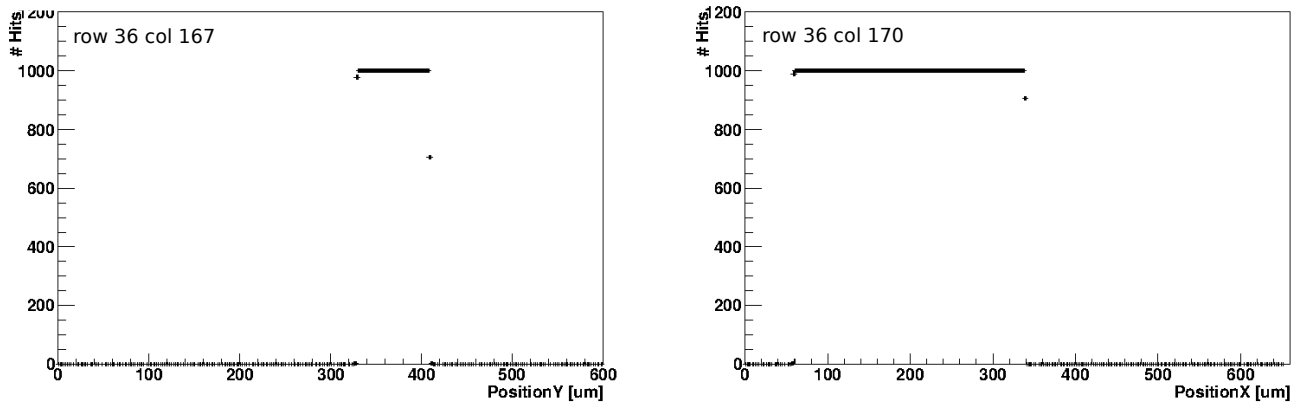


Figure 4.4.: The results for the y (left) and x (right) single measurements a single pixel. The number of trigger signals was set to 1000. The error for a measurement point x is \sqrt{x} .

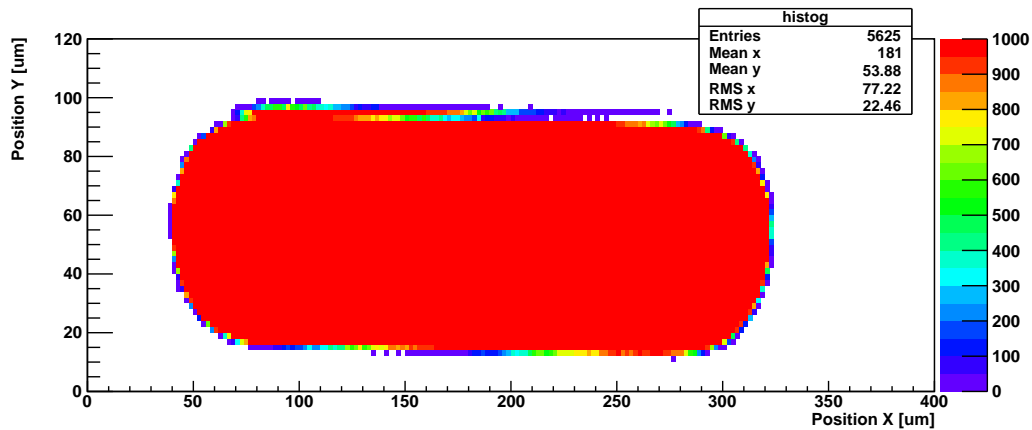


Figure 4.5.: The pixel (35/165) which was centered during the measurement over a whole pixel. The measurement was done with 1000 Events per scan point.

occupancy of 1000. To the border region the detected hits are decreased as expected since the laser spot only partially hits the pixel. From the figure it can be seen, that the size of the pixel is larger than expected ($250 \times 50 \mu\text{m}^2$). In the Figure 4.6, the overlap was investigated in detail. Here, the sum of the four affected pixels and the maximal entry is plotted against the position for the same region of the measurement point. In the upper Figure it is shown that, in the region between the pixels, more than one pixel is hit at the same time. This effect reaches from two pixels showing hits (green coloured) to three hit pixel (yellow coloured) until all four pixels show hits in the middle region (red coloured). The lower pictures shows the maximal value detected by all of the four pixels. This value is homogenous for the whole region.

4. Results

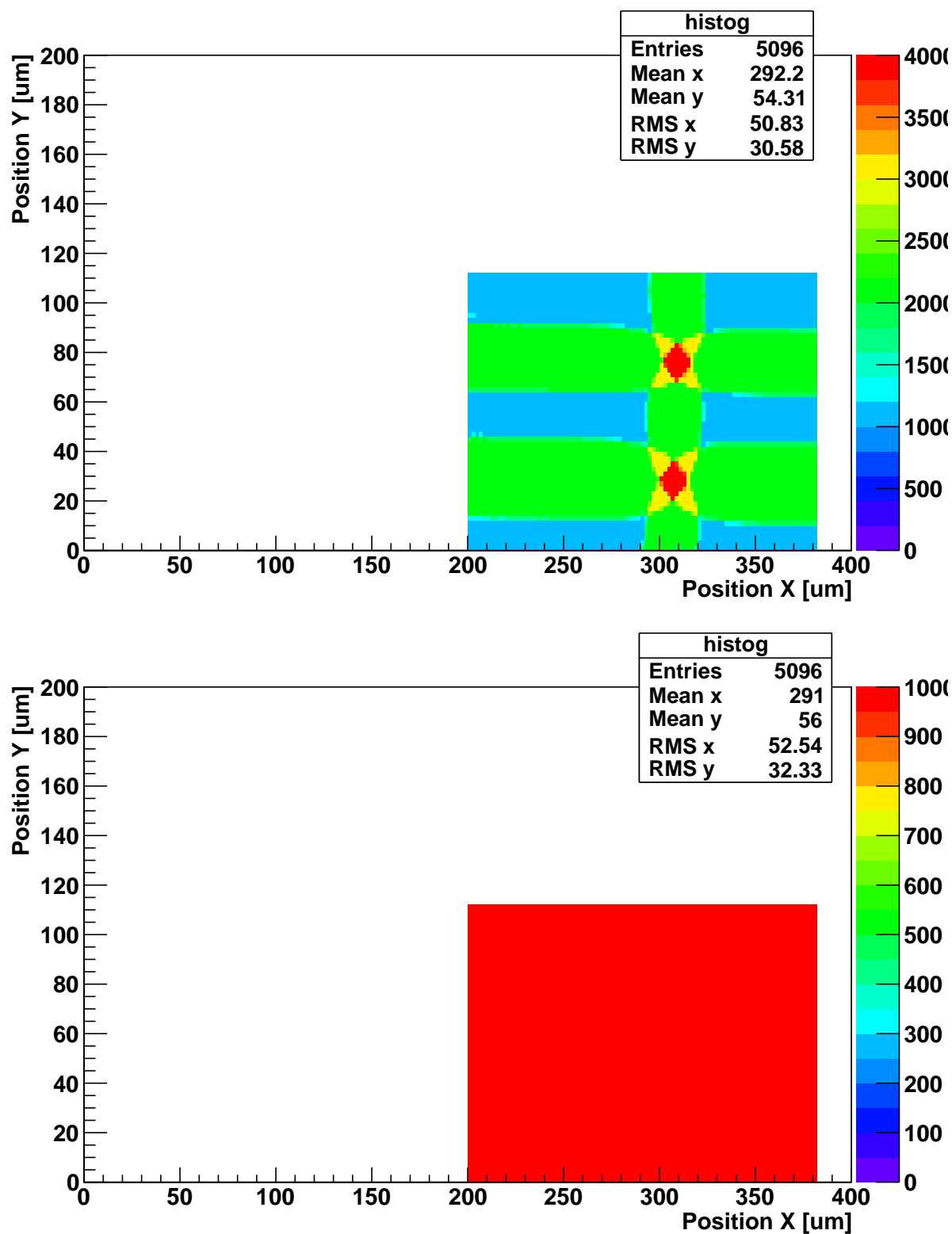


Figure 4.6.: The overlay of four different pixels. The upper picture shows the summed up occupancies, the lower one the maximum of the entries.

5. Discussion

In the following the results are analysed and discussed.

At first, it is to mention that the implemented functions work as mentioned. All position of the sensor can be reached moving the chuck or the microscope.

For the calculation of the diameter, it needs to be respected that the hit efficiency is not equal to one on the pixel and zero in front of and behind it [14]. This means that the pixel already shows hits even when the pixel is not yet reached or has already passed. To include this in the formula, the length D of the pixel needs to be replaced by the width of the charge distribution.

Furthermore, Figure 4.3 shows that the ToT is not a real plateau. There are deviations and a small decrease to the end of the pixel. For this reason, it is not absolute clear where the plateau is reached and so the determination of the point A , B and P is not well defined. To specify an error for this is difficult, since the behaviour is not the same in detail for the two measurements shown. A reason for this could be the charge sharing with neighbouring pixels. Since the diameter is in the order of $40\ \mu\text{m}$ and the width of a pixel is $50\ \mu\text{m}$, it is very likely to hit more than one pixel. This was not seen in the measurement for the diameter, but this just means that the threshold for the pixels was not yet reached. Because of the aberration of the alignment, this effect gets more likely to the end of the pixel. If it is assumed that the laser spot was located in the middle of the first pixel (35/165) the movement drifts more and more in the y direction to the next column. This explains why for the second pixel (34/165), the decrease is larger.

For the single measurements along one direction, the expected behaviour is seen. A sharp edge appears when the chip is reached. From then on, for every trigger signal a hit is detected. The comparatively small rising of the ToT shows that the full amount is not reached as sharply as the plots for the occupancy show. To get a hit in every trigger signal not the full laser spot needs to be located on the pixel, only for every trigger signal a hit needs to be detected but not all hits. For the ToT measurement, the maximal value is reached when the whole laser spot is located above the pixel. Since this process takes longer, the maximum is reached after more steps. For efficiency measurements the slow increase is advantageous since the edge of a pixel can be investigated in a more detailed

5. Discussion

view. Using Formular 3.1 for every ToT value, the injected amount of electrons can be calculated. The behaviour is therefore similar. The injected number of electrons is in order of the value expected (14,000) from the tuning of the configuration.

For the In-pixel measurement (Figure 4.5), it can be seen that the alignment was not perfect. On the top left or the bottom right of the pixel, the edge of the pixel is not sharp since for these x position the y position is not the same as for the positions before.

Towards the edges of the pixel the number decreases since a part of the laser spot is not positioned above the pixel. In addition, on the top side of the pixel two lines seem to be special (y position between 90 and 95), given that the upper one shows the maximal number of hits and the lower one already has a decreased signal. If the two lines would be swapped the Figure would correspond to the behaviour of the lower side. The reason for this is not clear but a miswriting of data cannot be excluded.

An influence of the bias dot cannot be seen. Since the size of the laser spot is nearly as large as the width of the pixel it is conceivable that even when the bias dot is hit, a large part of the sensor still records hits. As seen in the comparison of the occupancy and the ToT measurements, the region in which the number of hits would be decreased is very small (about $4 \mu\text{m}$). To investigate the influence of the bias dot the resolution has to be increased. The reason for the larger size of the shown pixel is the size of the laser spot (Figure 4.2).

If a Gaussian distributed laser intensity is assumed, since the laser is assumed to be equally distributed, even before and after the pixel is radiated by the whole laser spot, the full occupancy can be reached. Due to this, the pixel size d_P seems to be larger. If Δx is the part of the distribution sufficient to generate the maximal signal, the laser spot is seen in the size $d_s = d_P + 2\Delta x$. From the figure it follows that $d_s = 280 \pm 5 \mu\text{m}$ and therefore $\Delta x = 15 \mu\text{m}$. From this, a spot size of $d = 2\Delta x = 30 \mu\text{m}$ is calculated for a symmetric distribution.

In the Figure 4.6 the behaviour in the border region can be seen. The size of the laser spot results in an overlay of the different pixels. The start of the overlay is seen when the second pixel is hit, the end is reached when the first one is hit the last time. For two neighbouring pixels, the overlay is therefore equivalent to the spot size of the laser.

The cross in the upper Figure shows, that the edge region even between four pixels can clearly be seen. From the considerations mentioned before a laser spot size of $d = 30 \mu\text{m}$ can be read.

In the lower figure it can be seen, that on every position, even between all pixels, for every step the maximal number of hits is detected. This should be investigated with a higher resolution to decrease the region of the overlay. This is done by minimizing the diameter

of the laser spot. Due to this, in addition, the aberration of the movement becomes less important for a smaller diameter. If, e.g. for a diameter of $40\ \mu\text{m}$, the x axis is centered in the middle of a pixel and the deviation is $5\ \mu\text{m}$ by a movement of $100\ \mu\text{m}$ then the edge of the sensor and therefore the beginning of charge sharing is reached after $600\ \mu\text{m}$ movement. For a diameter of $30\ \mu\text{m}$ this point is reached after $700\ \mu\text{m}$ movement.

From reference [14], it can be seen that the diameter for the laser can be reduced to about $10\ \mu\text{m}$. To further investigate this, extra measurements need to be done with different diameters. The diameter is directly influenced by the focus of the microscope. In this thesis, the focus was done visually. A ToT measurement for different z positions of the microscope could be done over the edge of a pixel. From this, the diameter can be calculated as explained in Chapter 4.2.

As result of the thesis it can be said, that the efficiency measurements using laser injections have been enabled by using the implemented functions. Further measurements need to be done to investigate the behaviour of the pixels, especially on the bump pads and on the border regions.

A. Additional Plots

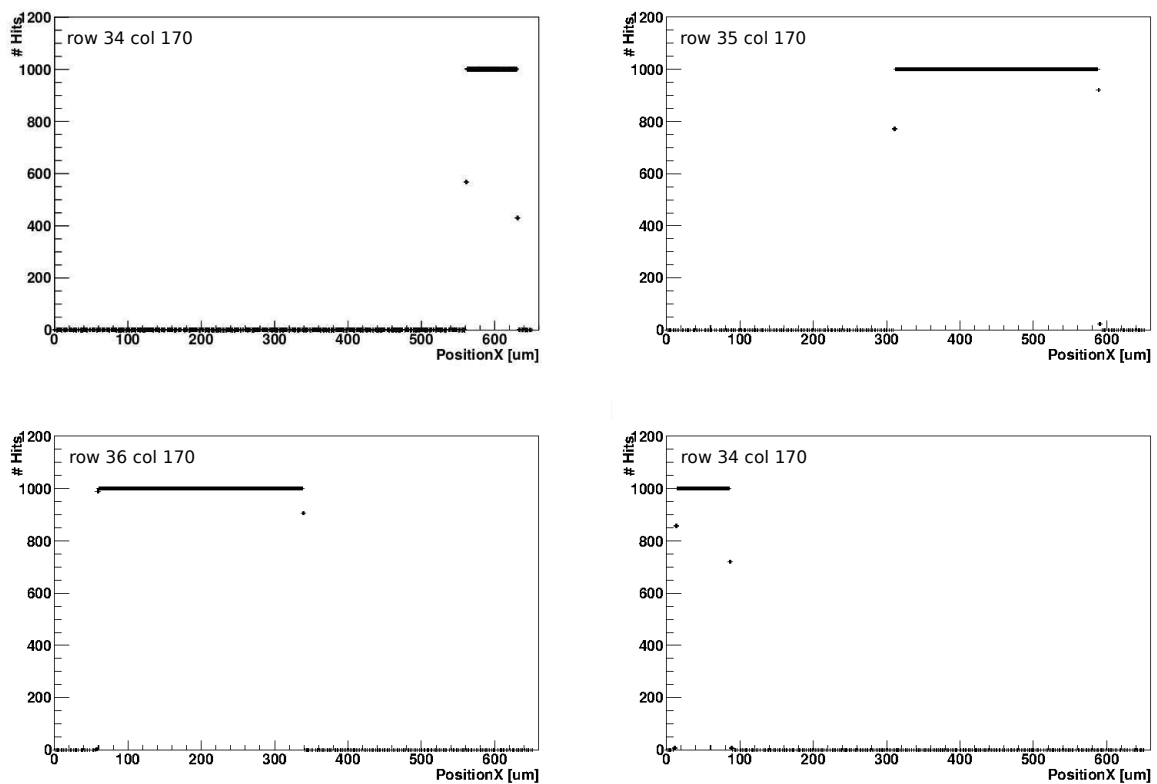


Figure A.1.: The results for the x direction measurements with $2 \mu\text{m}$ steps plotted for the single pixels. Comparing the pictures for neighbouring pixels an overlay can be seen.

A. Additional Plots

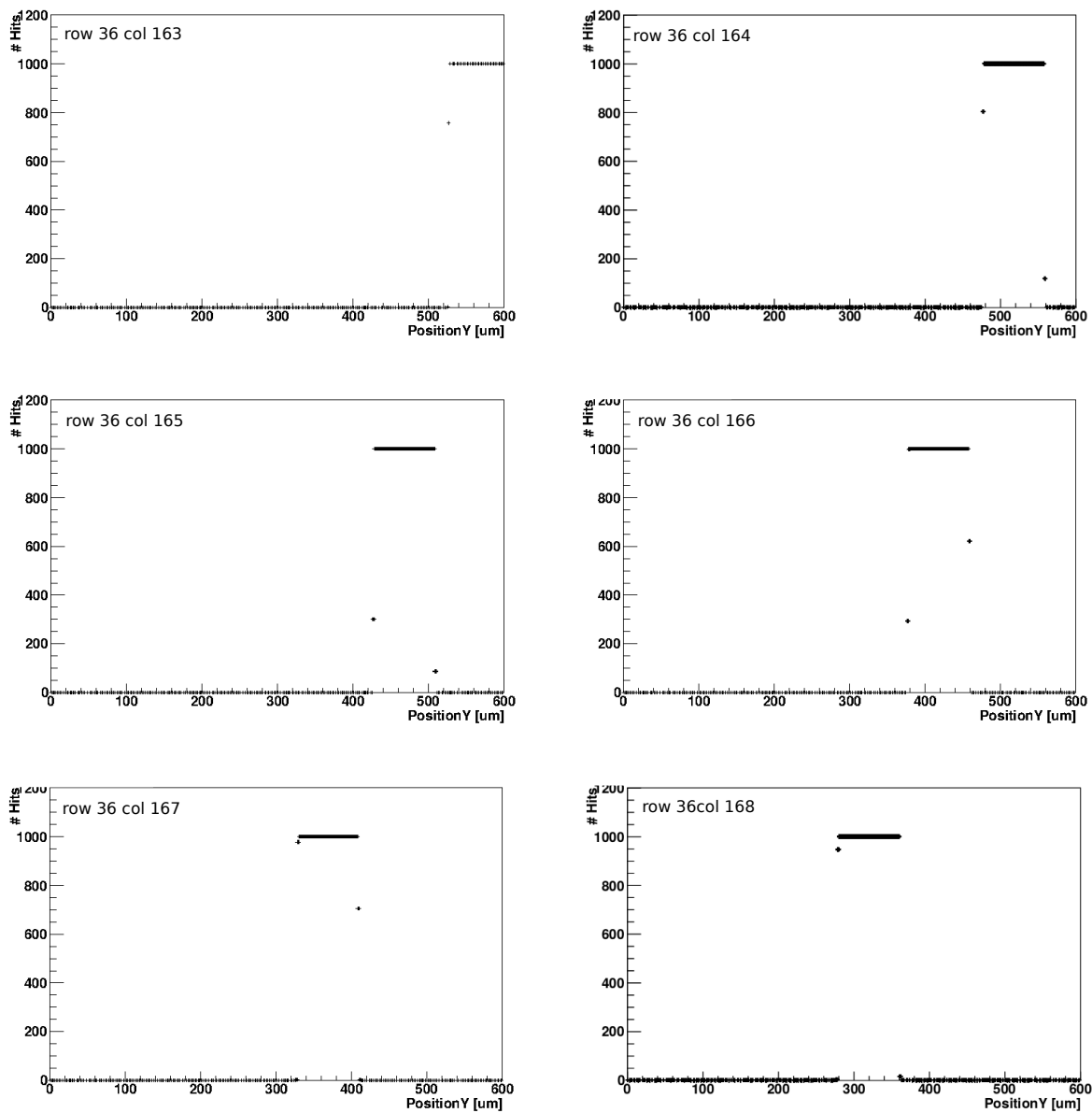


Figure A.2.: The results for the y direction measurements with 2 μm steps plotted for the single pixels. Comparing the pictures for neighbouring pixels an overlay can be seen.

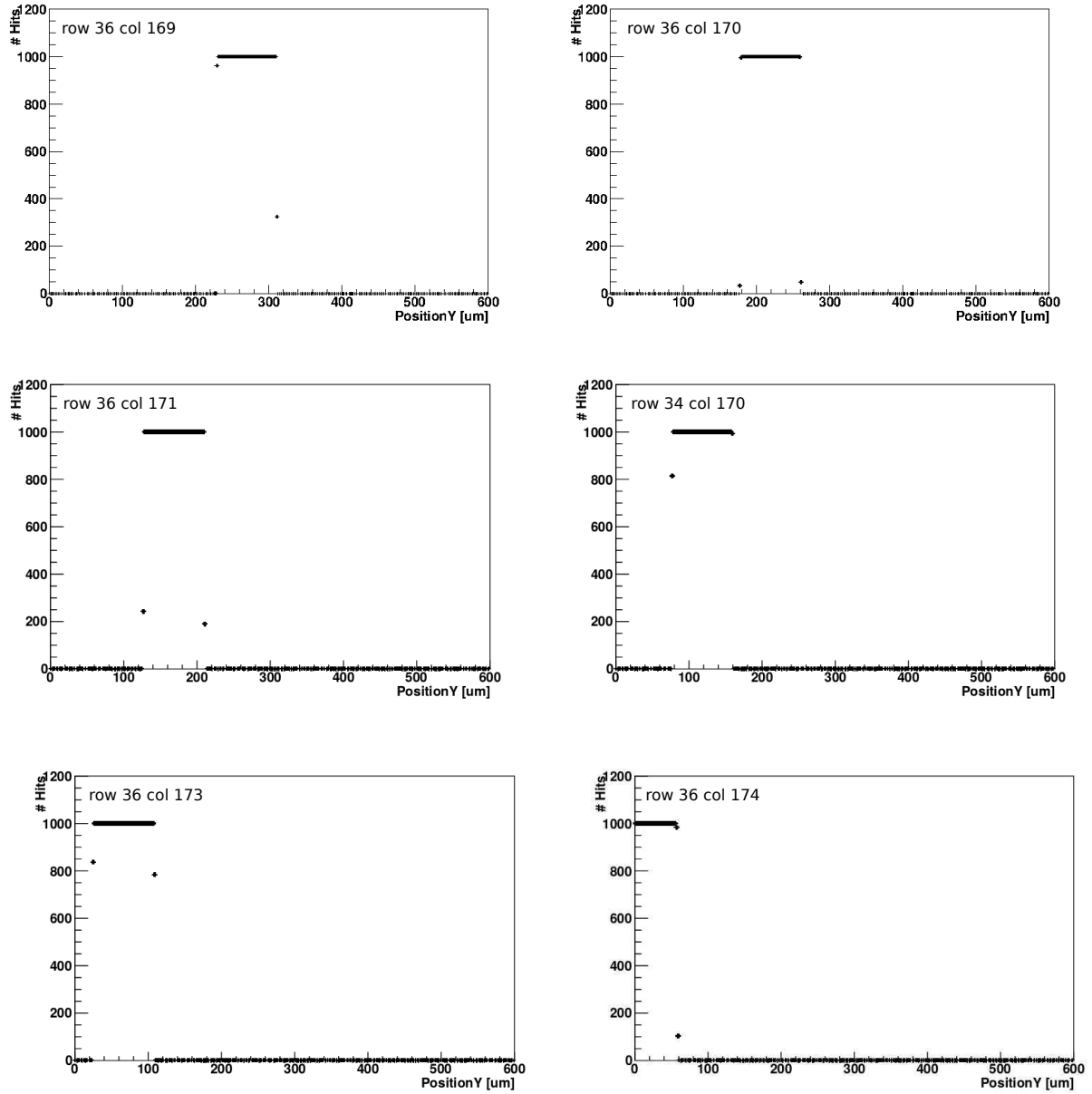


Figure A.3.: The results for the y direction measurements with $2 \mu\text{m}$ steps plotted for the single pixels. Comparing the pictures for neighbouring pixels an overlay can be seen.

Bibliography

- [1] O. Brüning et.al., *LHC Design Report Volume 1 The LHC Main Ring* (2008), Journal of Instrumentation (JINST) 3 S08003
- [2] C. Lefevre, *LHC the guide* (visited on June, 24th, 2014), CERN-Brochure-2009-003-Eng, cds.cern.ch/record/1165534
- [3] D. Cinca, *ATLAS Upgrades Towards the High Luminosity LHC: extending the discovery potential*, ATLAS Collaboration (2014), ATL-UPGRADE-PROC-2014-001
- [4] ATLAS Collaboration, *The ATLAS Experiment at the CERN Large Hadron Collider* (2008), Journal of Instrumentation (JINST) 3 S08003
- [5] C. Amsler, *Kern- und Teilchenphysik*, vdf Hochschulverlag AG (2007)
- [6] W. de Gruyter, *Bergmann Schaefer Lehrbuch der Experimentalphysik Band 4- Bestandteile der Materie* (2003), 2. Auflage
- [7] L. Rossi et.al., *Pixeldetectors-From Fundamentals to Applications*, Springer (2006)
- [8] Particle Data Group, *Review of Particle Physics* (2011), pdg.lbl.gov/2011/reviews/rpp2011-rev-passage-particles-matter.pdf
- [9] G. Lutz, *Semiconductor Radiation Detectors*, Springer (2001)
- [10] M. Capeans et.al., *ATLAS Insertable B-Layer Technical Design Report*, CERN-LHCC-2010-013
- [11] J. Rieger, *Comparison of Thin n- and p-type Bulk Silicon Pixel Sensors*, II. Physikalisches Institut Göttingen (2012), Master Thesis-II.Physik-UniGö-MSc-2012/08
- [12] FE-I4 Collaboration, *The FE-I4A Interated Circuit Guide Version 11.6*, ATLAS Experiment (2011)

Bibliography

- [13] *USBpix-USB based readout system for ATLAS FE-I3 and FE-I4*, <http://icwiki.physik.uni-bonn.de/twiki/bin/view/Systems/UsbPix> (visited on July 1st, 2014)
- [14] M. Pfaff, *Dynamic efficiency measurements for irradiated ATLAS Pixel single chip modules*, II. Physikalisches Institut Göttingen (2011), Diploma thesis

Danksagung

An dieser Stelle möchte ich mich bei allen bedanken, die mich während der Arbeit an meiner Bachelorarbeit unterstützt haben. Ein besonderer Dank gilt meinen Eltern, die mir nicht nur während der Bachelorarbeit, sondern auch während des gesamten Studiums den Rücken freigehalten haben und mich immer unterstützt haben. Vielen Dank.

Des weiteren danke ich Helen, die mich während der Arbeit unterstützt hat, besonders in stressigen Phasen.

Ich danke Prof. Dr. Arnulf Quadt der meine Arbeit im II. Physikalischen Institut ermöglicht und sich als Zweitgutachter zur Verfügung gestellt hat.

Ebenso danke ich PD Dr. Jörn Große-Knetter für die vielen hilfreichen Tipps während der Arbeit im Institut und die Bereitschaft, die Arbeit zu begutachten.

Ein ganz besonderer Dank gilt Julia und Johannes. Ohne euch wäre es mir nicht möglich gewesen die Aufgaben so schnell zu bewältigen. Ebenfalls danke ich euch für die fleißigen Korrekturen am Ende der Arbeitsphase und die vielen vielen hilfreichen Tipps zur Gestaltung der Arbeit.

Last but not least möchte ich mich bei der gesamten Hardware-Gruppe bedanken von denen jeder für Anregungen und Fragen zur Verfügung stand. Die Arbeit mit euch hat mir viel Spass gemacht.

Erklärung nach §13(8) der Prüfungsordnung für den Bachelor-Studiengang Physik und den Master-Studiengang Physik an der Universität Göttingen:

Hiermit erkläre ich, dass ich diese Abschlussarbeit selbständig verfasst habe, keine anderen als die angegebenen Quellen und Hilfsmittel benutzt habe und alle Stellen, die wörtlich oder sinngemäß aus veröffentlichten Schriften entnommen wurden, als solche kenntlich gemacht habe.

Darüberhinaus erkläre ich, dass diese Abschlussarbeit nicht, auch nicht auszugsweise, im Rahmen einer nichtbestandenenen Prüfung an dieser oder einer anderen Hochschule eingereicht wurde.

Göttingen, den October 13, 2014

(Fabian Sohns)